

Tensor Renormalization Group for interacting quantum fields

Manuel Campos, Germán Sierra and Esperanza López

Instituto de Física Teórica UAM/CSIC, C/ Nicolás Cabrera 13-15, Cantoblanco, 28049 Madrid, Spain

We present a new tensor network algorithm for calculating the partition function of interacting quantum field theories in 2 dimensions. It is based on the Tensor Renormalization Group (TRG) protocol, adapted to operate entirely at the level of fields. This strategy was applied in Ref.[1] to the much simpler case of a free boson, obtaining an excellent performance. Here we include an arbitrary self-interaction and treat it in the context of perturbation theory. A real space analogue of the Wilsonian effective action and its expansion in Feynman graphs is proposed. Using a $\lambda\phi^4$ theory for benchmark, we evaluate the order λ correction to the free energy. The results show a fast convergence with the bond dimension, implying that our algorithm captures well the effect of interaction on entanglement.

Tensor network techniques have been crucial to study strongly coupled spin systems relevant to condensed matter and statistical physics^{2–43}. The application of these techniques to quantum fields presents the challenge of dealing with infinite dimensional systems. Several strategies have been pursued to this aim. The most obvious is to introduce a truncation that brings back to the simpler framework of finite dimensional Hilbert spaces. An opposite philosophy has lead to the development of continuous versions of tensor networks^{44–51}. Tensor networks have also provided simple versions of the holographic principle within the AdS/CFT correspondence^{52–59}.

Inspired on standard field theory techniques, a different strategy was explored in¹. The main idea was to keep the continuous character of fields, treating them as the basic element for the implementation of an adapted Tensor Renormalization Group (TRG) protocol¹⁷. The viability of this approach was tested by evaluating the partition function of a free massive boson on a 2-dimensional square lattice. The results exhibited a very good numerical precision with moderate bond dimension, which in this case counts the number of fields per lattice link. Remarkably the massless limit could be addressed without an increase in the bond dimension.

The strength of the method relies on the combination of semi-analytic expressions and numerics that only involves finite dimensional matrices. This however is heavily based on the gaussian nature of free fields. Therefore it was an open question whether the same ideas are applicable to interacting field theories. We show that the answer is affirmative. Moreover, the semi-analytical character of the method exhibits important aspects of the interplay between interaction and entanglement.

The paper is organized as follows. We set the basis of our proposal in Section 1. Section 2 reviews the application to free fields. Section 3 contains a brief summary of the Wilsonian approach to quantum fields theories. Interaction is introduced in Section 4 in the context of perturbation theory. The structure of the TRG for interacting quantum fields is analyzed in Section 5. We explore the numerical performance of the protocol in Section 6. Section 7 presents a summary of results and discusses further lines of research. Technical details are consigned to appendices. An implementation in Mathematica of this adapted TRG network can be found in the GitHub repository⁶⁰.

I. A TENSOR NETWORK FOR QUANTUM FIELDS

The aim of this paper is to present a new framework for a real space renormalization group (RG) analysis of quantum field theories. It will combine the main guidelines of a conventional particle physics approach to quantum field theory^{61,62} with the introduction of a classification of degrees of freedom based on entanglement. The main focus of study will be the partition function, whose RG analysis will be formulated in terms of fields $x \in \mathbb{R}$. In the spirit of lattice field theory, the spacetime will be discretized.

We will work in two dimensions and consider a scalar field theory with Lagrangian

$$\mathcal{L} = \frac{1}{2}(\partial x)^2 + \frac{1}{2}m^2x^2 + \lambda v(x), \quad (1)$$

where m is the boson mass and λ a coupling constant. For concrete numerical evaluations we will choose $v(x) = x^4$, but otherwise we keep the potential generic. We will study a discretized version of this theory living on a square lattice with unit spatial and temporal steps. The field variables are assigned to the lattice links while the statistical or Boltzmann weights are carried by the vertices

$$\text{Diagram of a vertex on a square lattice. A central vertex is connected to four links. The top link is labeled } x_i. \text{ The vertex itself is labeled } W_0(x_i). \quad (2)$$

The weights $W_0(x_i)$ are given by

$$\begin{array}{c} 2 \\ | \\ 1 \text{---} 3 \\ | \\ 4 \end{array} = e^{-\frac{1}{2}\sum_{i=1}^4 [(x_i - x_{i+1})^2 + \frac{m^2}{2}x_i^2 + \lambda v(x_i)]}. \quad (3)$$

The partition function of the so defined vertex model is

$$Z = \int \prod_{i \in \text{links}} dx_i \times \prod_{j \in \text{vertices}} W_{0j}(x_i). \quad (4)$$

The evaluation of the partition function will be done by means of an adapted Tensor Renormalization Group protocol (TRG) that reduces iteratively the size of the lattice. The TRG for finite dimensional systems is based on the singular value decomposition (SVD) of the Boltzmann weights¹⁷

$$W = U_L D U_R^+, \quad (5)$$

where $U_{L,R}$ are unitary matrices, with U_R^+ denoting the adjoint of U_R , and D is a diagonal matrix containing the singular values of W . This decomposition has the following graphical representation

$$W = \text{---} \text{---} \text{---} \quad (6)$$

The tensor W can be analogously decomposed along the opposite diagonal. The variables in the new tilted links have a one to one correspondence with the singular values of W . Therefore they have a natural hierarchy based on entanglement. This allows to discard those with the weakest contribution. After the splitting (6) the old variables are summed over, eliminating degrees of freedom associated with short range entanglement. The number of lattice links is reduced in this process by a factor of two

$$\text{---} \text{---} \text{---} \Rightarrow \text{---} \text{---} \text{---} \Rightarrow \text{---} \text{---} \text{---} \quad (7)$$

Our proposal of a tensor network for quantum field theories can be summarized in a simple idea: apply the SVD splitting not to the Boltzmann weights, but to their exponent. This allows to treat fields as the basic elements, and to deal with finite tensors instead of functions while preserving the continuous character of the Boltzmann weights.

II. TRG FOR FREE FIELDS

Let W_n denote the Boltzmann weights of the discretized boson model at a given coarse graining level

$$\text{---} \text{---} \text{---} = W_n(\mathbf{x}_i) \quad (8)$$

where $\mathbf{x}_i = (x_{i1}, \dots, x_{i\chi_n})$ is the set of fields carried by each lattice link. We will refer to χ_n as the bond dimension of the tensor network. In analogy with (6), we are searching for a factorization of the form

$$W_n(\mathbf{x}_i) = \int d\mathbf{p} V_n(\mathbf{x}_1, \mathbf{x}_2; \mathbf{p}) V_n^+(\mathbf{p}; \mathbf{x}_4, \mathbf{x}_3) \quad (9)$$

The variables $\mathbf{p} = (p_1, \dots, p_{\chi_{n+1}})$, necessary for the splitting of W_n , are associated with the internal tilted link in (6). We require that $p_j \in \mathbb{R}$ in order to interpret them as fields. Thus χ_{n+1} will be the bond dimension of the new links. In this simple implementation of the TRG, x -fields on straight links and p -fields on tilted links alternate along the coarse graining iterations. The symmetries of the model allow to make a choice of basis for the fields such that all cubic weights, independently of their orientation, share the same expression. This choice has been assumed in (9).

A. Gaussian SVD

We consider first the implementation of this approach on the initial weights W_0 (3). The mass and interaction terms in the Lagrangian (1) do not contribute to the coupling of fields across lattice links. The only obstruction to a trivial splitting of W_0 is the factor

$$e^{-\frac{1}{2}[(x_2-x_3)^2+(x_1-x_4)^2]} \quad (10)$$

Remarkably a simple Fourier transform is enough to realise the scheme proposed in (9)

$$e^{-\frac{1}{2}(x_1-x_4)^2} = \frac{1}{\sqrt{2\pi}} \int dp_1 e^{ip_1(x_1-x_4) - \frac{1}{2}p_1^2} \quad (11)$$

An analogous expression holds for the mixing between $x_{2,3}$ after introducing a second splitting field p_2 . Hence the bond dimension is doubled in this process. While a single field lives at the links of the original lattice, $\chi_0 = 1$, the new tilted links carry two, $\chi_1 = 2$.

This simple mechanism is enough for the real space RG analysis of free field theories¹. In the absence of interaction, the weights (3) are gaussian. The splitting (11) respects this property. We can thus write the Boltzmann weights at any coarse graining level n as

$$W_n(\mathbf{x}) = F_n e^{-\frac{1}{2}\mathbf{x} M_n \mathbf{x}}, \quad (12)$$

with M_n a $4\chi_n \times 4\chi_n$ matrix and F_n a numerical factor. From now on boldface symbols without indices will denote collectively all fields involved in the expression under consideration. The argument of the Boltzmann weights are x -type fields for n even and p -type fields for n odd. For convenience and without loss of generality we have chosen the former to write down the general expression (12). A basis can be chosen¹ where M_n has the form

$$M_n = \begin{pmatrix} A_n & 0 \\ 0 & A_n \end{pmatrix} + \begin{pmatrix} B_n & -B_n \\ -B_n & B_n \end{pmatrix}, \quad (13)$$

where A_n and B_n are real, non-negative, symmetric matrices, and M_n acts on $\mathbf{x} = (\mathbf{x}_1, \mathbf{x}_2, \mathbf{x}_4, \mathbf{x}_3)$. For the initial weights W_0 the previous matrices are given by

$$A_0 = \begin{pmatrix} 1 & -1 \\ -1 & 1 \end{pmatrix} + \frac{m^2}{2} \mathbb{1}_2, \quad B_0 = \mathbb{1}_2 \quad (14)$$

The 2×2 block structure of (13) reflects the LR factorization that we need to implement in order to move to the next coarse graining level. With respect to the splitting (6), we have $\mathbf{x} = (\mathbf{x}_L, \mathbf{x}_R)$ with $\mathbf{x}_L = (\mathbf{x}_1, \mathbf{x}_2)$ and $\mathbf{x}_R = (\mathbf{x}_4, \mathbf{x}_3)$. Generalizing (10), the piece of the Boltzmann weights responsible for LR mixing is

$$e^{-\frac{1}{2}(\mathbf{x}_L - \mathbf{x}_R) B_n (\mathbf{x}_L - \mathbf{x}_R)} \quad (15)$$

Because of the mentioned properties of B_n , its SVD reduces to $B_n = U_n D_n U_n^T$ with U_n an orthogonal matrix. Using this

decomposition, we can apply again a Fourier transformation to rewrite (15) as

$$\frac{1}{\sqrt{(2\pi)^{\chi_{n+1}} \det D_n}} \int d\mathbf{p} e^{i(\mathbf{x}_L - \mathbf{x}_R) U_n \mathbf{p} - \frac{1}{2} \mathbf{p} D_n^{-1} \mathbf{p}}, \quad (16)$$

which implements the desired factorization. The splitting fields \mathbf{p} are in one to one correspondence with the singular values of B_n . In this way the TRG machinery is moved from the Boltzmann weights to their exponent, where fields are treated as the basic elements.

We add for completeness the expression of V_n

$$\begin{array}{c} \mathbf{x} \\ | \\ \text{---} \end{array} \begin{array}{c} | \\ \mathbf{p} \\ | \end{array} = f_n e^{-\frac{1}{2} \mathbf{x} A_n \mathbf{x} + i \mathbf{x} U_n \mathbf{p} - \frac{1}{4} \mathbf{p} D_n^{-1} \mathbf{p}}. \quad (17)$$

It holds for cubic weights with any of the four possible orientations. The normalization constant f_n is defined by the relation

$$F_n = \rho_n f_n^2, \quad \rho_n = \sqrt{(2\pi)^{\chi_{n+1}} \det D_n}. \quad (18)$$

This factorization mechanism was named gaussian SVD¹. In Appendix A we analyze the relation between the gaussian and the standard SVD, which for the Boltzmann weights (12) can be carried out explicitly. We show that the latter is also governed by the singular values of the matrix B_n . Therefore the gaussian SVD is not a different way of evaluating the LR mixing, which the standard SVD has been proved to do in an optimal way. Instead it provides a method to organize the infinite set of singular values obtained when working with continuous functions, grouping them into a finite number of subsets associated with fields.

We include a summary of the first two steps of the TRG

$$\begin{array}{c} \begin{array}{c} W_0 \\ | \\ \text{---} \end{array} \xrightarrow{\text{SVD}_0} \begin{array}{c} | \\ V_0 \\ | \end{array} = \begin{array}{c} \mathbf{x} \\ | \\ \text{---} \end{array} \begin{array}{c} | \\ \mathbf{p} \\ | \end{array} \chi_1 = 2 \\ \downarrow \\ \begin{array}{c} \text{---} \end{array} \begin{array}{c} \mathbf{x} \\ | \\ \text{---} \end{array} \begin{array}{c} | \\ \mathbf{p} \\ | \end{array} \chi_2 = 2 \xleftarrow{\text{SVD}_1} \begin{array}{c} W_1 \\ \times \\ \mathbf{p} \end{array} \xleftarrow{\int d\mathbf{x}} \begin{array}{c} \text{---} \end{array} \begin{array}{c} \mathbf{x} \\ | \\ \text{---} \end{array} \begin{array}{c} | \\ \mathbf{p} \\ | \end{array} \\ \downarrow \\ \begin{array}{c} \text{---} \end{array} \begin{array}{c} \mathbf{x} \\ | \\ \text{---} \end{array} \begin{array}{c} | \\ \mathbf{p} \\ | \end{array} \xrightarrow{\int d\mathbf{p}} \begin{array}{c} | \\ W_2 \\ | \end{array} \end{array} \quad (19)$$

The singular value matrices D_{2n+1} turn out to have half of their diagonal entries equal to zero. The would be splitting fields associated with them can be readily discarded. As a consequence, the bond dimension doubles when evolving from x -fields to p -fields but keeps constant from p to x -fields¹. Therefore

$$\chi_{2n} = 2^n. \quad (20)$$

B. Numerical results

The free energy per site of the discretized free boson model

$$f = -\frac{1}{N} \log Z, \quad (21)$$

where N is the number of lattice sites and Z is the partition function (4), was used to test the numerical performance of this adapted TRG protocol¹. The coarse graining process trades space time degrees of freedom by link variables. The exponential increase in the bond dimension that (20) describes is not numerically sustainable. Truncation was implemented by discarding small singular values of the LR mixing matrix B_n , together with their associated splitting fields. Fig.1 shows the results obtained with different maximal number of fields per link. An average precision of 10^{-8} was achieved with $\chi_{\max} = 64$ across a wide range of boson masses. Remarkably no increase in the bond dimension was necessary to access small masses. This allowed to evaluate the central charge of the CFT emerging in the massless limit. The value $c = 1$ was reproduced to within a 10^{-5} error.

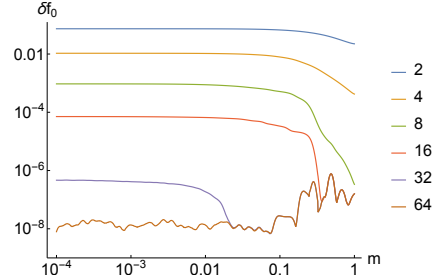


Figure 1. Relative error in the free energy per site, $\delta f = \frac{f_{\text{TRG}} - f_{\text{ex}}}{f_{\text{ex}}}$, as a function of the boson mass for different maximal bond dimensions. A lattice with $N = 2^{40}$ sites has been considered, such that the exact free energy f_{ex} can be replaced by its $N \rightarrow \infty$ limit.

It was also proven that the coarse graining process attains an infrared fixed point at the right length scale set by the boson mass, even for small bond dimension. Recall that each field encodes an infinite subset of the singular values resulting from a standard SVD, described in (A16). This subset contains arbitrarily small entries, which might explain why working in terms of fields retains relevant long distance information for any bond dimension.

III. THE EFFECTIVE ACTION

The treatment of interaction will be inspired in the standard approach to quantum field theories. Searching for numerical efficiency is not our only motivation. We aim at obtaining new insights based on entanglement, and for that it is convenient to make a natural connection with the commonly used techniques and concepts.

We will start reviewing some basic facts about effective field theories^{61,62}. Let us consider a theory defined at a ultraviolet (UV) momentum scale Λ by the Lagrangian (1). The

partition function of the theory is given by

$$Z = \int_{[0,\Lambda]} \mathcal{D}\phi e^{-S[\phi]}, \quad S[\phi] = \int d\xi \mathcal{L}[\phi], \quad (22)$$

where the variables ξ_i denote spacetime directions. Let $\Lambda' < \Lambda$ be a smaller scale. The field ϕ contains *slow* modes with a momentum smaller than Λ' , and *fast* modes with momentum in the interval $[\Lambda', \Lambda]$. We denote them as $\phi_<$ and $\phi_>$ respectively. The action $S[\phi]$ can be divided into a quadratic part S_0 , and S_1 which collects the interaction terms

$$S[\phi_<, \phi_>] = S_0[\phi_<] + S_0[\phi_>] + \lambda S_1[\phi_<, \phi_>]. \quad (23)$$

Quadratic cross terms between $\phi_<$ and $\phi_>$ have been disregarded because these fields are orthogonal upon integration. Replacing (23) into (22) and integrating the fast modes yields

$$Z = \int \mathcal{D}\phi_< e^{-S_{eff}[\phi_<]}. \quad (24)$$

where $S_{eff}[\phi_<] = S_0[\phi_<] + S_{int}[\phi_<]$ is the Wilsonian effective action at the scale Λ' . The term S_{int} is derived from the expectation value of S_1 taken with the quadratic action of the fast fields

$$e^{-S_{int}[\phi_<]} = \int \mathcal{D}\phi_> e^{-S_0[\phi_>] - \lambda S_1[\phi_<, \phi_>]}. \quad (25)$$

When λ is small, the average (25) can be evaluated by means of a perturbative expansion. Its contribution to the effective action at each order in λ is described by a sum of connected Feynman diagrams whose internal lines are $\phi_>$ propagators. We use double lines for $\phi_>$ propagators and solid lines for $\phi_<$ external legs. Feynman diagrams will be depicted in red for avoiding confusion with the tensor network structure of the discretized model. Taking as example a $\lambda \phi^4$ theory, some diagrams at second order in perturbation theory are



$$. \quad (26)$$

The integration of high momentum modes gives rise to terms with any number of external legs.

IV. TRG FOR INTERACTING QUANTUM FIELDS

Guided by the previous formulation, we search for a real space RG protocol that can be implemented by local operations. Namely, we want the partition function to be given at each coarse graining level n by

$$Z = \int \prod_{i \in \text{links}} d\mathbf{x}_i \times \prod_{j \in \text{vertices}} W_{n,j}(\mathbf{x}). \quad (27)$$

For concreteness we have chosen x -type fields to write down this general expression. The Boltzmann weights W_n should depend only on the fields living at contiguous links, as in (12).

The product

$$\prod_{j \in \text{vertices}} W_{n,j}(\mathbf{x}), \quad (28)$$

is the real space analogue of the Wilsonian effective action, with n playing the role of the UV cutoff Λ' . Preserving the structure of (12), we define

$$W_n(\mathbf{x}) = e^{-\frac{1}{2} \mathbf{x} M_n \mathbf{x}} F_n(\mathbf{x}). \quad (29)$$

The matrix M_n encodes all λ -independent quadratic terms, being the counterpart of $\mathcal{L}_0[\phi_<]$. The function F_n contains the effects of interaction and therefore relates to $S_{int}[\phi_<]$.

A. Real space Feynman diagrams

We analyze in this Section the new features introduced by interaction, focussing in the first TRG iteration. The initial weights W_0 of the discretized interacting model were given in (3). The matrix M_0 is constructed from A_0 and B_0 in (14), and the function F_0 is

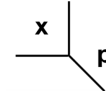
$$F_0(\mathbf{x}) = e^{-\frac{\lambda}{2} \sum_{i=1}^4 v(x_i)}, \quad (30)$$

with $\mathbf{x} = (x_1, \dots, x_4)$. The dependence of F_0 on x_i trivially factorizes. Anticipating the LR splitting needed to move to the next coarse graining level, we define

$$F_0(\mathbf{x}) = \rho_0 f_0(\mathbf{x}_L) f_0(\mathbf{x}_R), \quad (31)$$

where \mathbf{x}_L labels the fields at two contiguous links entering W_0 and \mathbf{x}_R those at the other two complementary links. A constant ρ_0 has been introduced for convenience as in (18). It is the normalization factor of the Fourier transform (16), which in this case equals 2π .

Following Section II.B for the factorization of the gaussian cross terms in W_0 , the resulting cubic weights are



$$= e^{-\frac{1}{2} \mathbf{x} A_0 \mathbf{x} + i \mathbf{x} \mathbf{p} - \frac{1}{4} \mathbf{p}^2} f_0(\mathbf{x}). \quad (32)$$

The exponential prefactor reproduces (17) after taking into account that, since $B_0 = \mathbb{1}_2$, its SVD data U_0 and D_0 are also the identity. Sewing together four cubic weights as shown in (19) and integrating out the original \mathbf{x} fields, we obtain



$$= \text{four-point vertex diagram}, \quad (33)$$

which stands for

$$W_1(\mathbf{p}) = e^{-\frac{1}{4} \mathbf{p}^2} \int d\mathbf{x} e^{-\frac{1}{2} \mathbf{x} Q_0 \mathbf{x} + i \mathbf{x} C_0 \mathbf{p}} \prod_{i=1}^4 f_0^{(i)}(\mathbf{x}). \quad (34)$$

The matrices Q_0 and C_0 , of dimensions 4×4 and 4×8 respectively, are readily constructed from A_0 and U_0 . Their concrete expressions can be found in Appendix B.

The gaussian kernel of (34) can be further simplified by the change of variables

$$\mathbf{x} \rightarrow \mathbf{x} + i Q_0^{-1} C_0 \mathbf{p}. \quad (35)$$

It leads to the structure (29) for W_1 with

$$M_1 = \frac{1}{2} \mathbb{1}_8 + C_0^T Q_0^{-1} C_0 . \quad (36)$$

The first term on the *rhs* reproduces the gaussian factor in front of the integral (34), and the second is generated by the previous shift of variables. The function F_1 encoding the effects of interaction is given by

$$F_1(\mathbf{p}) = \int d\mathbf{x} e^{-\frac{1}{2}\mathbf{x}Q_0\mathbf{x}} \prod_{i=1}^4 f_0^{(i)}(\mathbf{x} + iQ_0^{-1}C_0\mathbf{p}) . \quad (37)$$

This expression can be considered a local analogue of (25), with \mathbf{x} and \mathbf{p} identified with the fields $\phi_>$ and $\phi_<$ respectively. We can therefore evaluate F_1 with the same tools used for the effective action. In particular, we might use a perturbative expansion when the coupling constant is small.

Order by order in λ the integral (37) is gaussian and can be easily performed. This is done by considering all possible pairings of the x_i variables and replacing

$$x_i x_j \rightarrow (Q_0^{-1})_{ij} , \quad (38)$$

which is equivalent to the well known Wick's theorem. The matrix Q_0^{-1} plays the role of the high momentum mode propagator. Using this, a set of Feynman rules can be defined in terms of which to construct the real space analogue of Feynman diagrams. This is presented in Appendix C. The logarithm of F_1 is given by a sum of so defined connected Feynman diagrams. For a $\lambda\phi^4$ theory, schematically we will have

$$\log F_1 \propto 1 - \lambda \left(\text{8} + \text{O} + \text{X} \right) + \dots \quad (39)$$

We have followed the same graphical notation as in (26): a double line for the original fields \mathbf{x} , living at the four inner links on the *lhs* of (33), and a single line for the first level fields \mathbf{p} , carried by the four tilted links.

B. Interacting SVD

The effects of interaction on the TRG protocol appear after the first coarse graining integration. Contrary to F_0 , the function F_1 does not satisfy the trivial factorization (31). This is an immediate consequence of the matrix Q_0 not being diagonal.

The non-factorization of F_1 is to be expected, since the contrary will imply that interaction has no effect on entanglement. As a consequence of this, the LR splitting protocol has to be revisited. To that aim we consider the following function of two variables, which serves as a simplified version of the general weights (29)

$$e^{-\frac{b}{2}(x-y)^2} F(x, y) . \quad (40)$$

The parameter b represents a singular value of the LR mixing matrix B (15). The function F is assumed to be symmetric

under the exchange of x and y , but otherwise arbitrary. This is consistent with the symmetries of the lattice model. Although F does not satisfy in general (31), it can be rewritten as

$$F(x, y) = \rho f(x, z) f(y, -z) , \quad z = x - y , \quad (41)$$

for some appropriate but not unique function f . A possible although not necessarily convenient choice of f is

$$f(x, z) = \sqrt{\rho^{-1} F(x, x - z)} . \quad (42)$$

Recall the main guidelines of the TRG protocol that we wish to design. First, obtaining an SVD-like protocol that classifies *fields* according to an entanglement criterium. Second, keeping the coarse graining process *local*. This requires that no residual coupling between x and y , linked to the function F , remains after splitting. We will start by analyzing how the transformation (11) fails to meet the latter condition. Upgrading z in (41) into an independent field, the general expression (40) can be restated as

$$\frac{\rho}{2\pi} \int dz dp e^{ip(x-y-z) - \frac{b}{2}z^2} f(x, z) f(y, -z) . \quad (43)$$

Integrating p produces a delta function that imposes $z = x - y$, and equality immediately follows. Let us invert the order of integration and evaluate first the integral in z

$$\frac{\rho}{2\pi} \int dz e^{-ipz - \frac{b}{2}z^2} f(x, z) f(y, -z) . \quad (44)$$

The functions f are brought out of the integral by promoting them into a the differential operator

$$\hat{f}(x, \partial_p) = f(x, z)|_{z=i\partial_p} . \quad (45)$$

The gaussian integral can then be explicitly evaluated. We set $\rho = \sqrt{2\pi b}$ such that numerical factors cancel, and obtain

$$\hat{f}(x, \partial_p) \hat{f}(y, -\partial_p) e^{-\frac{1}{2b}p^2} . \quad (46)$$

When f is independent of z , as in (31), the standard Fourier transform is recovered. In the general case, the fact that both differential operators act on the same gaussian factor hinders factorization.

This problem has a simple solution. We may double the splitting fields such that each differential operator acts on a different gaussian factor. This is achieved by considering

$$F(x, y) = \tilde{\rho} f(x, z^1) f(y, -z^2) , \quad z^{1,2} = x - y , \quad (47)$$

with $\tilde{\rho} = \rho^2/2$. We upgrade again $z^{1,2}$ into independent variables with the help of two Fourier fields $p^{1,2}$. Using this trick (40) can be factorized as follows

$$\int dp^1 dp^2 V(x; p^1, p^2) V^*(y; p^2, p^1) , \quad (48)$$

with

$$V(x; p^1, p^2) = e^{ix(p^1 + p^2)} \left(\hat{f}(x, \partial_{p^1}) e^{-\frac{(p^1)^2}{b}} \right) . \quad (49)$$

Notice that V depends on both splitting fields, albeit in an asymmetrical manner.

C. Feynman diagrams and SVD

We have seen that the function F_1 encoding the interaction effects of the level one Boltzmann weights, admits a diagrammatic expansion. We analyze here how this feature behaves under the factorization protocol.

Recall that the first TRG iteration exchanges the roles of the x and p variables. Following (47), we define

$$F_1(\mathbf{p}_L, \mathbf{p}_R) = \tilde{\rho}_1 f_1(\mathbf{p}_L, \mathbf{z}^1) f_1(\mathbf{p}_R, -\mathbf{z}^2), \quad (50)$$

with $\tilde{\rho}_1$ an appropriate constant and

$$\mathbf{z}^1 = \mathbf{z}^2 = \mathbf{p}_L - \mathbf{p}_R. \quad (51)$$

In order to understand the structure of f_1 , we focus on a simple example. Let us consider a contribution to F_1 of the form

$$e^{-\lambda(\mathbf{p}_L \cdot \mathbf{p}_R)^2}. \quad (52)$$

The argument of the exponential represents a connected Feynman diagram with four legs contributing at first order in perturbation theory. It has the same structure as the last graph in (39). The splitting of the previous term according to (50) is

$$e^{-\frac{\lambda}{2}[\mathbf{p}_L \cdot (\mathbf{p}_L - \mathbf{z}^1)]^2} e^{-\frac{\lambda}{2}[\mathbf{p}_R \cdot (\mathbf{p}_R + \mathbf{z}^2)]^2}. \quad (53)$$

We observe that the four leg diagram is inherited by both factors. The coefficient weighting the diagram has been modified such that the original term is recovered when substituting (51). The undesired dependence on the fields $\mathbf{p}_{L,R}$ has been replaced with the help of the auxiliary variables $\mathbf{z}^{1,2}$.

The previous example illustrates a general conclusion. Connected Feynman diagrams in the expansion of F_1 reappear in f_1 with their topological structure unchanged. Therefore, since the former has a diagrammatic expansion so it does the latter. As shown in (39) the logarithm of F_1 only contains connected Feynman diagrams. Expression (53) makes clear that this property is also inherited by f_1 . By induction, these statements hold at all coarse graining levels.

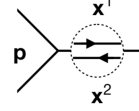
V. INTERACTION AND ENTANGLEMENT

The semi-analytical character of the coarse graining protocol that we have designed allows to obtain interesting results on the interplay between interaction and entanglement already before addressing its numerical implementation. That will be the subject of this Section.

A. A tale of two fields

We are ready to factorize the level one Boltzmann weights. As explained above, two sets of splitting fields $\mathbf{x}^{1,2}$ are necessary. Upper indices will always make reference to the splitting

process. The resulting cubic weight $V_1(\mathbf{p}; \mathbf{x}^1, \mathbf{x}^2)$ is



$$V_1(\mathbf{p}; \mathbf{x}^1, \mathbf{x}^2) = e^{-\frac{1}{2} \mathbf{p} A_1 \mathbf{p} + i \mathbf{p} U_1 (\mathbf{x}^1 + \mathbf{x}^2)} \times \left(\hat{f}_1(\mathbf{p}, \partial_{\mathbf{x}^1}) e^{-\mathbf{x}^1 D_1^{-1} \mathbf{x}^1} \right). \quad (54)$$

Generalizing (45), the differential operator \hat{f}_1 is given by

$$\hat{f}_1(\mathbf{p}, \partial_{\mathbf{x}^1}) = f_1(\mathbf{p}, \mathbf{z})|_{\mathbf{z}=iU_1 \partial_{\mathbf{x}^1}}. \quad (55)$$

The matrices A_1 , U_1 and D_1 governing the gaussian terms are those already present in the free case (17).

The arrows in the magnified link stress the different roles that the fields $\mathbf{x}^{1,2}$ play in the cubic weight. This is better understood by considering the linear combinations

$$\bar{\mathbf{x}} = \mathbf{x}^1 + \mathbf{x}^2, \quad \hat{\mathbf{x}} = \mathbf{x}^1 - \mathbf{x}^2. \quad (56)$$

We will refer to them as even and odd variables respectively. The λ -independent coupling of \mathbf{p} with the splitting fields only involves the even variables $\bar{\mathbf{x}}$. In the absence of interaction the odd variables $\hat{\mathbf{x}}$ completely decouple, since multiplying contributions from the L and R cubic weights we have

$$e^{-\mathbf{x}^1 D_1^{-1} \mathbf{x}^1 - \mathbf{x}^2 D_1^{-1} \mathbf{x}^2} = e^{-\frac{1}{2} \bar{\mathbf{x}} D_1^{-1} \bar{\mathbf{x}} - \frac{1}{2} \hat{\mathbf{x}} D_1^{-1} \hat{\mathbf{x}}}. \quad (57)$$

Therefore $\bar{\mathbf{x}}$ is the counterpart of the splitting fields already present in the gaussian SVD, while $\hat{\mathbf{x}}$ allows to treat locally the new entanglement ties created by interaction. Without interaction the latter become trivial.

Sewing four cubic weights (54) and following the steps presented in Section IV.A for the elimination of \mathbf{p} , we obtain the second level Boltzmann weights

$$W_2(\mathbf{x}) = e^{-\frac{1}{2} \mathbf{x} M_2 \mathbf{x}} F_2(\mathbf{x}). \quad (58)$$

Here \mathbf{x} stands for both splitting fields $(\bar{\mathbf{x}}, \hat{\mathbf{x}})$. Recall that the gaussian prefactor only contains leading terms in the perturbative expansion, namely $\mathcal{O}(\lambda^0)$. Its exponent is given by

$$\mathbf{x} M_2 \mathbf{x} = \bar{\mathbf{x}} \left(\frac{1}{2} S_1 + C_1^T Q_1^{-1} C_1 \right) \bar{\mathbf{x}} + \frac{1}{2} \hat{\mathbf{x}} S_1 \hat{\mathbf{x}}, \quad (59)$$

with $S_1 = \mathbb{1}_4 \otimes D_1^{-1}$ diagonal, and Q_1 and C_1 constructed out of A_1 and U_1 respectively as explained in Appendix B. The expression in parenthesis is the same combination governing the level one Boltzmann weights in the absence of interaction. This shows the direct connection between $\bar{\mathbf{x}}$ and the fields already present in the free network. We have disregarded quadratic terms between even and odd variables. Indeed, relation (57) implies that they trivially cancel in the product of Boltzmann weights (28) building up the partition function.

The effect of interaction is encoded in the function

$$F_2(\mathbf{x}) = e^{\mathbf{u} S_1 \mathbf{u}} \hat{\mathcal{F}}_2(\bar{\mathbf{x}}, \partial_{\mathbf{u}}) e^{-\mathbf{u} S_1 \mathbf{u}}|_{\mathbf{u}=\mathbf{x}^1}. \quad (60)$$

A variable \mathbf{u} has been introduced in order to unambiguously define the action of the derivatives inherited from \hat{f}_1 . The differential operator $\hat{\mathcal{F}}_2(\bar{\mathbf{x}}, \partial_{\mathbf{u}})$ is given by

$$\int d\mathbf{p} e^{-\frac{1}{2} \mathbf{p} Q_1 \mathbf{p}} \prod_{i=1}^4 \hat{f}_1^{(i)}(\mathbf{p} + i Q_1^{-1} C_1 \bar{\mathbf{x}}, \partial_{\mathbf{u}}). \quad (61)$$

This integral is the level one equivalent of (37). The expression (60) may seem unconventional. It is however reminiscent of the Hermite polynomials

$$H_n(x) = (-1)^n e^{x^2} \frac{d^n}{dx^n} e^{-x^2}. \quad (62)$$

Each monomial x^k in H_n is to be related with a Feynman diagram with k external legs of type **u**. This introduces an additional structure in the set of Feynman diagrams, whose relevance we discuss below.

B. General structure

The main feature of our protocol is the introduction of new fields representing the effect of interaction on entanglement. They first appear at the second coarse graining level, corresponding to the odd combination of the splitting fields.

We recall schematically the leading order structure of the even and odd fields, $\bar{\mathbf{x}}$ and $\hat{\mathbf{x}}$ respectively, using the decomposition (13) of M_2

$$A_2 = \begin{pmatrix} A_{2\bar{\mathbf{x}}} & 0 \\ 0 & A_{2\hat{\mathbf{x}}} \end{pmatrix}, \quad B_2 = \begin{pmatrix} B_{2\bar{\mathbf{x}}} & 0 \\ 0 & 0 \end{pmatrix}. \quad (63)$$

The decoupling between even and odd variables, together with the vanishing of the odd mixing matrix $B_{2\hat{\mathbf{x}}}$, shows the trivial nature of $\hat{\mathbf{x}}$ at leading order $\mathcal{O}(\lambda^0)$. Namely, these fields just represent decoupled degrees of freedom living at each link. However they contribute in general to LR mixing through the function F_2 , and require an own set of splitting fields to continue the coarse graining process.

In the simplified splitting problem (40), the vanishing of $B_{2\hat{\mathbf{x}}}$ is equivalent to setting $b = 0$. It is thus a question whether the factorization technique of Section III.B applies in this limiting situation, which moreover will be recurrent in subsequent iterations. In order to clarify this point we send b to zero in (49), after renaming the splitting fields as $q^{1,2}$. The product of the gaussian exponential and its associated normalization factor ρ results then in a delta function

$$\lim_{b \rightarrow 0} \frac{1}{\sqrt{\pi b}} e^{-\frac{1}{b}(q^1)^2} = \delta(q^1). \quad (64)$$

Namely, the consequence of a vanishing b is the collapse into a delta function of the probability distribution of q^1 . In the free case, a delta function implies that the associated field can be trivially removed from the coarse graining process. In the presence of interaction, this does not hold anymore.

We come back to the factorization of $W_2(\mathbf{x})$. The splitting fields for the even and odd variables $\bar{\mathbf{x}}$ and $\hat{\mathbf{x}}$ will be denoted by \mathbf{p} and \mathbf{q} respectively. As just explained, the probability distribution of fields \mathbf{q} collapses into a delta function. The level two cubic weights are then

$$\begin{array}{c} \mathbf{x} \\ \swarrow \quad \searrow \\ \mathbf{p}^1, \mathbf{q}^1 \end{array} = e^{-\frac{1}{2}\mathbf{x}A_2\mathbf{x} + i\bar{\mathbf{x}}U_2\bar{\mathbf{p}} + i\hat{\mathbf{x}}\bar{\mathbf{q}}} \times \quad (65)$$

$$\hat{f}_2(\mathbf{x}, \partial_{\mathbf{p}^1}, \partial_{\mathbf{q}^1}) \left(e^{-\mathbf{p}^1 D_2^{-1} \mathbf{p}^1} \delta(\mathbf{q}^1) \right),$$

with U_2 and D_2 the SVD data of $B_{2\bar{\mathbf{x}}}$. The differential operator \hat{f}_2 induces derivatives of $\delta(\mathbf{q}^1)$. The delta derivatives can not be evaluated right away. This has to be postponed to the coarse graining integral that eliminates \mathbf{q} . It will be done using integration by parts, which is equivalent to work at the level of the Hermite polynomials (62) instead of dealing with individual Feynman diagrams. In this way the fields \mathbf{q} , in spite of their singular distribution function, provide a regular and well defined contribution to the propagation of entanglement.

Due to the need of doubling the splitting fields, the bond dimension of the TRG network with interaction increases twice as fast as in the free case. However the different roles of the even and odd combinations in perturbation theory induce a clear distinction between fields. A reduced set of them will be in direct correspondence with the fields already present in the free network, inheriting from them their leading order structure. This set is given by

$$\mathbf{x}_{(0)} \rightarrow \mathbf{p}_{(1)} \rightarrow \bar{\mathbf{x}}_{(2)} \rightarrow \bar{\mathbf{p}}_{(3)} \rightarrow \bar{\mathbf{x}}_{(4)} \rightarrow \dots \quad (66)$$

where the index in parenthesis labels the coarse graining level. Hence $\bar{\mathbf{x}}_{(2)}$ refers to the corresponding fields in (59) and $\bar{\mathbf{p}}_{(3)}$ to those in (65). The dots stand for the even combination of splitting fields associated with the previous term in the chain.

The largest set of fields represents entanglement ties created by interaction. At each coarse graining level a new family of them is seeded by the odd counterpart of the variables (66)

$$\begin{array}{l} \hat{\mathbf{x}}_{(2)} \begin{cases} \bar{\mathbf{q}}_{(3)} \equiv \bar{\mathbf{p}}_{(2,3)} \leftarrow \dots \\ \hat{\mathbf{q}}_{(3)} \equiv \hat{\mathbf{p}}_{(2,3)} \leftarrow \dots \end{cases} \\ \hat{\mathbf{p}}_{(3)} \leftarrow \dots \end{array} \quad (67)$$

In order to stress the structure organizing this set of fields, we have renamed \mathbf{q} in (65) as $\mathbf{p}_{(2,3)}$. All these fields have a trivial leading order structure, as $\hat{\mathbf{x}}_{(2)}$ in (59). Many of them will have a singular distribution function, as it is the case of $\mathbf{p}_{(2,3)}$, but this does not represent a harm for the TRG protocol.

C. A perturbative bound on χ

In the previous section we have not made reference to the order at which we want the perturbative expansion to stop. This is however an important information for the TRG protocol, which sets a limit to the propagation of entanglement mediated by odd variables and results in a reduction of the large set of extra fields (67).

For $n \geq 2$ it is best to analyze the effects of the interaction in terms of a differential operator $\hat{\mathcal{F}}_n(\bar{\mathbf{x}}, \partial_{\mathbf{u}})$, generalizing $\hat{\mathcal{F}}_2$

in (60) and defined by an integral as in (61)

$$\hat{\mathcal{F}}_n(\bar{\mathbf{x}}, \partial_{\mathbf{u}}) = \text{Diagram} \quad (68)$$

Recall that \mathbf{u} is an auxiliary variable which, after the evaluation of the derivatives, should be replaced by \mathbf{x}^1 introducing therefore a dependence on the odd variables. The operator $\hat{\mathcal{F}}_n$ admits an expansion in Feynman graphs, where the graphs's external legs can carry components of the vector $\bar{\mathbf{x}}$ or the derivative $\partial_{\mathbf{u}}$. Let us assume that in order to move to the next coarse graining level we factorize (68) along the axis $i : (1, 2)_L - (3, 4)_R$. A generic connected diagram in the expansion of $\hat{\mathcal{F}}_n$ has the structure

$$\text{Diagram} \quad (69)$$

The subgraph on the left originates from $\hat{f}_{n-1}^{(1,2)}$ and contributes m_L powers of the coupling constant. A corresponding statement holds for the subgraph on the right. After introducing the necessary splitting fields, the previous graph will be inherited by the cubic weights resulting from the factorization of (68) as described in Section IV.C. Appendix D proves that splitting fields associated with the odd variables $\hat{\mathbf{x}}$, such as $\mathbf{q}^{1,2}$ in (66), are only required in diagrams satisfying

$$m_L, m_R \geq 1, \quad m_L + m_R \leq N, \quad (70)$$

with N the order at which to cut the perturbative expansion.

Clearly these conditions cannot be met at first order in perturbation theory. Although doubling the splitting fields is necessary, at first order in λ the odd combinations represent short range entanglement and their effect extinguishes within one iteration

$$\begin{array}{ccccccc} \mathbf{x}_{(0)} & \rightarrow & \mathbf{P}_{(1)} & \rightarrow & \bar{\mathbf{x}}_{(2)} & \rightarrow & \bar{\mathbf{P}}_{(3)} & \rightarrow & \bar{\mathbf{x}}_{(4)} & \rightarrow & \dots \\ & & \searrow & & \searrow & & \searrow & & \searrow & & \\ & & \hat{\mathbf{x}}_{(2)} & & \hat{\mathbf{P}}_{(3)} & & \hat{\mathbf{x}}_{(4)} & & \dots & & \end{array} \quad (71)$$

The upper row contains the fields (66) with a counterpart in the free network. From the set (67) only the first item in each tree is relevant. This drastic simplification is consistent with the rather trivial nature of quantum corrections at order λ .

At second order in perturbation theory (70) implies

$$m_L = m_R = 1. \quad (72)$$

Thus if a Feynman diagram contributes to odd variable mixing in the n -th iteration, it will not do it at any subsequent one. Indeed, as an individual diagram it fails to satisfy the first condition (70), while as part of a larger diagram it will be the second which fails. The fields involved at second order include (71), plus secondary chains with that same structure stemming from each element of the second row. Namely the second level odd fields, such as $\hat{\mathbf{p}}_{(2,3)}$ in (67), get extinguished

within one iteration at second order in λ . It is straightforward to generalize this reasoning to order N , with the result that at larger N more ramifications in (67) become relevant. Equivalently, high orders in perturbation theory require a growing number of extra fields to represent locally the effects of interaction. We consider this property a consistency check of our proposal.

We shall end with a comment on the fields (66). It was mentioned in Section II.A that before truncation kicks in, the singular values matrices D_{2n+1} have half of their diagonal entries equal to zero. The probability distribution of the associated fields is thus a delta function. Although in the free case these fields are trivially discarded, in the presence of interaction some of them become relevant and need to be kept. We show in Appendix E that this only happens when conditions (70) are met. Since these extra fields behave with respect to the perturbative order as the odd variables do, we will not discuss them further.

VI. NUMERICAL RESULTS

In the previous sections we have extended the TRG protocol based on local operations formulated in terms of fields to include interactions. We will start here the analysis of its numerical performance using as benchmark a $\lambda\phi^4$ theory. This theory has been studied with tensor networks techniques which imply the discretization of the field variables in^{26,35,40,43,58}.

A. Truncation

The last question that needs to be addressed before implementing the TRG is truncation. In the free case truncation consists in discarding small singular values of the matrix B_n . As (64) shows, this is equivalent to approximate the probability distribution of the splitting fields related with small singular values by a delta function.

Perturbation theory treats in an asymmetrical way quadratic terms and interaction, giving rise to a potential problem. Truncation is only justified for fields with small LR cross terms from *both* the leading order gaussian prefactor and the Feynman diagrams. This only represents a problem for fields contributing non trivially at leading and higher order in λ , namely, the set (66). These two conditions are a priori not related, since fields with a delta function distribution can yet have a relevant contribution to Feynman diagrams via delta derivatives. Checking their compatibility is the first issue in the numerical study of the TRG. We will work below at first order in perturbation theory to simplify the analysis by focussing as much as possible on the set (66).

When the TRG protocol is applied at first order in λ , there is one-to-one correspondence between the leading order gaussian structure of the even fields, and their counterpart in the free network. See Appendix E for details. Since the odd fields do not contribute to the propagation of entanglement, they play a secondary role. Motivated by this we will apply the term bond dimension to the number of fields in (66), which

without truncation is given by (20). As for the criterium of truncation, we will adopt the simplest choice and base it again on the singular values of B_n .

B. Partition function

We present the results on the numerical evaluation of the free energy per site of a $\lambda\phi^4$ theory

$$-\frac{1}{N} \log Z = f_0 + \lambda f_1 + \mathcal{O}(\lambda^2). \quad (73)$$

Fig.2 shows the relative error in the first order correction f_1 for several maximal bond dimensions and masses. The relative error of the leading term f_0 is also included for comparison. A remarkable feature of the TRG protocol is the capacity to correctly estimate f_0 in the massless limit without varying the bond dimension. This property however does not extend to f_1 , which requires a sustained increase in the bond dimension to keep the precision as the mass lowers. On the other hand, the convergence with χ_{\max} appears to be faster for f_1 than for f_0 . Notice that the precision in f_1 improves on that of f_0 down to $m \approx 0.06$ with just $\chi_{\max} = 20$.

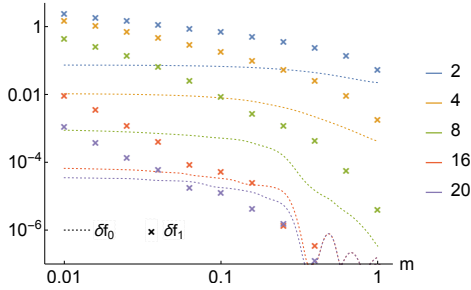


Figure 2. Relative errors δf_0 (dotted lines) and δf_1 (crosses) in the free energy per site as a function of the mass and the bond dimension, in a lattice of size $N = 2^{40}$.

It is important to quantify the convergence of the TRG with the bond dimension. The error in the leading term of the free energy at fixed mass follows a power law, $(\chi_{\max})^{-\alpha}$. This is observed in Fig.3a, where choosing as example $m = 0.1$ and setting $\alpha = 3.7$ we have obtained a very good fit of δf_0 . The behaviour of δf_1 is plotted in Fig.3b at the same mass. The error for small bond dimension, although larger than that of the leading term, decreases exponentially fast. As the precision improves, the dependence on χ_{\max} turns into a power law with exponent $\alpha = 7.3$. This confirms the faster convergence of δf_1 across all bond dimensions. A similar pattern holds at other values of the mass. The smaller the mass, the bigger the error at fixed bond dimension and the larger the range of χ_{\max} where convergence is exponential.

In the same way that the singular values of B_n describe the entanglement hierarchy at leading order, new quantities are needed to characterize how interaction modifies it. To this aim we will use the cubic weights, V_n . After the maximal bond dimension is reached, they result from the factorization of the

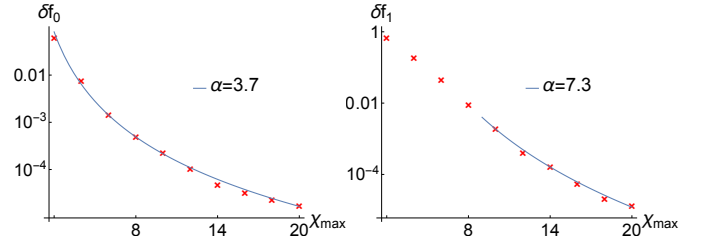


Figure 3. Relative errors a) δf_0 and b) δf_1 as a function of the bond dimension at $m = 0.1$. The blue lines represent a power law fit $(\chi_{\max})^{-\alpha}$.

Boltzmann weights plus a truncation guided by the matrix B_n

$$\begin{array}{c} \chi_{\max} \\ | \\ \text{---} \end{array} \Rightarrow \begin{array}{c} \chi_{\max} \\ | \\ \text{---} \end{array} \begin{array}{c} \chi_{\max} \\ | \\ \text{---} \end{array} \begin{array}{c} \chi_{\max} \\ | \\ \text{---} \end{array} \quad (74)$$

We will be interested in the cubic weights *before* implementing the truncation represented in second step. At first order in the coupling constant, V_n can be written as

$$\begin{array}{c} \mathbf{x} \\ | \\ \text{---} \end{array} \begin{array}{c} \mathbf{p}^1 \\ | \\ \text{---} \end{array} \begin{array}{c} \mathbf{p}^2 \\ | \\ \text{---} \end{array} = e^{-\frac{1}{2} \bar{\mathbf{x}} (A_n - \frac{1}{2} \mathbb{1}_2 \otimes D_{n-1}^{-1}) \bar{\mathbf{x}} + i \bar{\mathbf{x}} U_n \bar{\mathbf{p}}} \times \quad (75)$$

$$\left[\hat{g}_n (\partial_{\mathbf{p}^1}, \bar{\mathbf{x}}, \partial_{\mathbf{u}}) e^{-\mathbf{u} (\mathbb{1}_2 \otimes D_{n-1}^{-1}) \mathbf{u} - \mathbf{p}^1 D_n^{-1} \mathbf{p}^1} \right]_{\mathbf{u}=\mathbf{x}^1}.$$

The $\chi_{\max} \times \chi_{\max}$ matrix D_{n-1} and the $2\chi_{\max} \times 2\chi_{\max}$ matrices A_n , U_n and D_n are precisely the same as in the free case. Upon evaluating the derivatives $\partial_{\mathbf{u}}$, the differential operator \hat{g}_n will transform into the level n generalisation of (55).

For a $\lambda\phi^4$ theory, the operator \hat{g}_n can be represented in the terms of the quartic polynomial

$$c_n \left[1 + \lambda \left(T_n^{(0)} + \sum_{i,j} T_{n,ij}^{(2)} z_i z_j + \sum_{i,j,k,l} T_{n,ijkl}^{(4)} z_i z_j z_k z_l \right) \right], \quad (76)$$

where the vector \mathbf{z} stands for $(\partial_{\mathbf{p}^1}, \bar{\mathbf{x}}, \partial_{\mathbf{u}})$. The leading order constant c_n has been factored out in the definition of the order- k tensors $T_n^{(k)}$. Using these tensors we define

$$\omega_{n,i}^{(2)} = \frac{1}{\chi_{\max}} \sum_j |T_{n,ij}^{(2)}|, \quad \omega_{n,i}^{(4)} = \frac{1}{\chi_{\max}^3} \sum_{jkl} |T_{n,ijkl}^{(4)}|, \quad (77)$$

with $i = 1, \dots, 2\chi_{\max}$ running over the components of $\partial_{\mathbf{p}^1}$. These quantities provide an estimate of the relevance of p_i^1 in transmitting the effect of interaction. The larger the bond dimension, the smaller are some of the singular values in the diagonal matrices D_n . If the derivatives $\partial_{\mathbf{u}}$ and $\partial_{\mathbf{p}^1}$ in (75) were evaluated, small singular values would induce artificially large entries in the previous tensors. Such large contributions just mean that the probability distribution of the associated fields is close to a delta function and, as discussed above, the TRG protocol can deal with these objects.

The singular values of B_n and the above defined ω 's are plotted in Fig.4a for $m = 0.1$ at the coarse graining level $n = 8$.

We observe that the singular values follow a marked descending pattern. On the contrary the ω 's start slightly increasing and reach then a plateau extending up to $i \simeq 10$. This implies that interaction strengthens the first set of entanglement ties, tending to make them equally relevant. However, although the entanglement hierarchy is modified, it is not incompatible with the leading order truncation criterium based on B_n . Indeed, the entries $\omega_{n,i}$ with $i > 14$ present a clear decreasing trend. The associated splitting fields can thus be discarded with a small error both at the level of the leading and first order terms. This is in agreement with the good performance of $\chi_{\max} = 16$ for $m = 0.1$ seen in Fig.2. It is interesting to notice the similarity between the ω 's related to the two and four leg tensors.

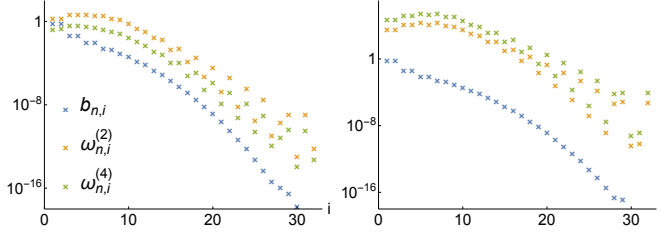
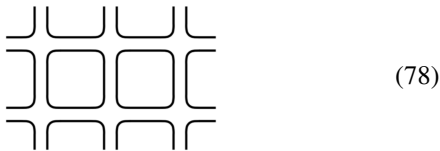


Figure 4. Singular values of B_n and sum of tensor elements (77) for a) $m = 0.1$ and b) $m = 0.01$ at the coarse graining level $n = 8$. The number of b 's and ω 's at that level is $2\chi_n = 32$.

The behaviour shown in Fig.4a is general. Moreover, the smaller the mass the more ω 's should be taken into account to obtain a good precision. This is observed in Fig.4b, which suggests that including up to $i \simeq 20$ is necessary to reasonably describe the first order effects when $m = 0.01$. The pattern of the ω 's also explains the two regimes seen in Fig.3b, exponential and power law, for the dependence of the relative error δf_1 on the bond dimension. Only when χ_{\max} is large enough to include all fields associated with similarly relevant values of ω , the convergence changes from exponential to power law. On the other hand, the singular values of B_n for $m = 0.1$ and 0.01 practically coincide. This agrees with the almost equal leading order error δf_0 seen in Fig.2 for both masses.

C. CDL structure

The standard TRG has the drawback of not being fully able to eliminate short range entanglement²². The infrared (IR) fixed point of gapped systems treated with this protocol is given by a so-called corner double line structure (CDL)



Correlations in the CDL network are confined inside each plaquette. A SVD based coarse graining fails however to detect this structure and promotes half of the CDL loops to the next level. This problem is replicated by the free boson TRG¹.

Indeed the RG flow of the gaussian weights (12) can be described by the evolution

$$M_n \rightarrow M_{CDL}, \quad (79)$$

where the only non-zero entries of the matrix M_{CDL} are those described by the CDL vertex.

When the degrees of freedom running in each plaquette decouple from the others, it is simple to integrate them out. In this sense the CDL is nothing but a redundant way to represent a trivial IR fixed point. This is confirmed by the ability of the TRG to transform the free boson lattice into a CDL network as the coarse graining process surpasses the scale set by the boson mass¹. Having into account that the lattice spacing doubles every two TRG iterations, this happens when

$$n > 2 \log_2 m^{-1}. \quad (80)$$

We show in Fig.5a the RG evolution of the singular values of B_n for $\chi_{\max} = 16$ and $m = 0.01$. At $n \simeq 18$ half of the singular values start to strongly decay. This signals the emergence of a CDL structure, since contributions from fields at opposite corners trivially factorize. At the same time the CDL matrix (79) freezes out, which is also observed in that figure. The value $n = 18$ is in good agreement with the theoretical estimation (80), whose *rhs* for $m = 0.01$ gives 13.3. Notice that the quotient between the correlation length, $\xi \simeq m^{-1}$, and the lattice spacing at $n = 18$ is $\simeq 0.2$.

We are ready now to analyze the RG flow associated with the first order correction to the free energy. The tensors defined in (76) encode the structure at first order in the perturbative expansion of the $\lambda \phi^4$ theory. They should reach an IR fixed point at the same scale as the singular values $b_{n,i}$. A modification of the IR scale (80) can only arise from an all order resummation of perturbative effects, as that implied by the usual RG equations. We are not addressing this issue here. Consistently, we found that the two and four leg tensors freeze out right after the leading gaussian structure reaches the CDL fixed point.

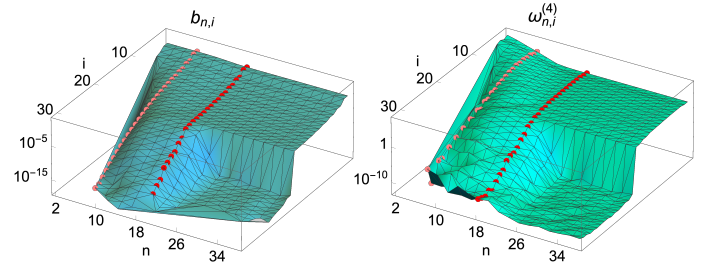


Figure 5. RG flow of a) the singular values of B_n and b) the sum of $T_n^{(4)}$ elements (77) for $\chi_{\max} = 16$ and $m = 0.01$. The pink line signals $n = 8$, the iteration where truncation begins with $\chi_{\max} = 16$, and the red line marks $n = 18$. These plots refer n even, horizontal lattices. Analogous results describe n odd, tilted lattices.

The RG flow of the order λ terms can be portrayed with the help of (77). We have plotted in Fig.5b the evolution of the ω 's associated with $T_n^{(4)}$ for $\chi_{\max} = 16$ and $m = 0.01$. Not only these quantities stabilise at the same time as $b_{n,i}$, but together with them, the corresponding half becomes zero. The

same result holds for $T_n^{(2)}$. This implies that the associated \mathbf{p} in (75) are irrelevant to the factorization of both gaussian and interacting cross terms. Hence the truncation in the second step of (74) is automatic, which is a distinct characteristic of the CDL structure.

Finally, we have checked that the two and four leg tensors reproduce the CDL pattern of network connections. To that aim we define the matrix

$$\Omega_{ij} = |T_{n,ij}^{(2)}| + \frac{1}{\chi_{\max}^2} \sum_{k,l} |T_{n,ijkl}^{(4)}|. \quad (81)$$

Recall that its indices refer to $(\partial_{\mathbf{p}^1}, \bar{\mathbf{x}}, \partial_{\mathbf{u}})$. Contrary to (77), we assume that the truncation in the second step of (74) has been already implemented and the bond dimension in all links is χ_{\max} . A non-zero entry Ω_{ij} reflects that the Feynman diagrams connect components i and j . A graphical representation of this matrix is given in Fig.6 for $\chi_{\max} = 16$, $m = 0.01$ and $n = 24$, when the CDL regime is clearly established for the leading gaussian terms. The boxes defined by the thin black lines have dimension $\chi_{\max} \times \chi_{\max}$, while the numbers on their side label the links of the CDL cubic weight included in that figure. The colour code describes the magnitude of the entries, making clear the CDL structure. We obtain thus a unified picture of the RG flow at leading and first order in the coupling constant.

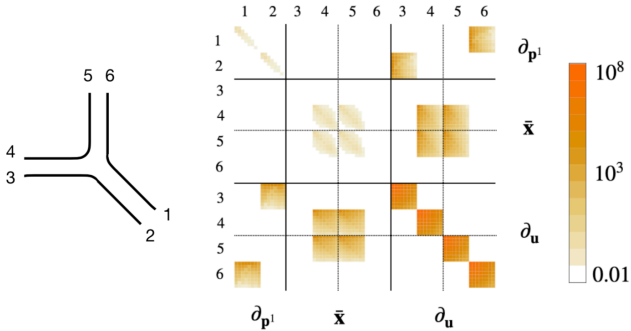


Figure 6. Colour plot of the matrix (81) for $\chi_{\max} = 16$, $m = 0.01$ and $n = 24$.

VII. CONCLUSIONS

We have explored the formulation of a real space coarse graining protocol for interacting QFT's based on local manipulations on continuous variables. Together with an entanglement rooted organisation of degrees of freedom, we have used the standard Wilsonian approach as guideline. This led to move the SVD analysis characteristic of real space RG algorithms from the Boltzmann weights, which describe the discretized QFT partition function, to their exponent or in other words, to the free energy. Our motivation was to operate directly at the level of fields. Each field is a proxy for an infinite subset of the singular values that would result from a standard SVD. The strong structure that this automatically implies aims

to be an efficient theoretical tool, able to obtain insights that are difficult for more numerical oriented algorithms.

We have developed a framework based on the TRG network¹⁷, which realises this program in the context of perturbation theory. Describing the effect of interaction in terms of local manipulations requires the introduction of extra fields with distinct properties. They have a trivial leading order structure and their number increases with the order in perturbation theory at which we want to work. Due to the simple nature of the associated quantum corrections, the role of these additional fields at first order in the coupling constant is secondary. It would be therefore important to extend the detailed numerical analysis we have performed here beyond first order.

The adapted TRG network evaluates the partition function of a free boson with excellent precision and a numerical cost independent of the boson mass¹. We have chosen a $\lambda\phi^4$ theory to benchmark the performance at first order in perturbation theory. In this case the numerical cost increases at small masses, but the results exhibit a fast convergence with the bond dimension. Using the direct correspondence between the field content of the free and first order networks, we have analyzed how the interaction modifies the leading order entanglement hierarchy. The quantum corrections work towards levelling off the pattern of marked decreasing relevance that organizes the fields in the absence of interaction. This effect involves a larger subset of fields the lower the mass is, explaining a dependence of the numerical cost on the mass which was not present in the free network. Besides, we obtained a consistent picture of the RG flow at leading and first order. As it is characteristic of standard TRG algorithms, a fixed point with CDL structure was attained in the IR.

Tensor networks are designed to deal with any value of the coupling constant. The perturbative approach we have followed here might seem thus limited. We believe however that it is an important step towards a goal that is extremely difficult for QFT. Although beyond the scope of this paper, a venue to include non-perturbative effects could be adding finite λ corrections to the gaussian structure that underlies the algorithm. A modification of the leading order gaussian structure can also be relevant for improving the performance in the limit of small masses. On the other hand, we would like to stress that the perturbative framework is not essential for the SVD protocol presented in Section IV.B.

Finally, there are other interesting and simpler generalizations of the adapted TRG protocol. In particular, the calculation of correlation functions and its application to field theories with fermions. We plan to address some of these issues in the near future.

ACKNOWLEDGMENTS

We thank Pasquale Calabrese, José Melgarejo, Javier Molina-Villaplana, Giuseppe Mussardo, Antoine Tilloy and Erik Tonni for conversations. The work of M.C. is supported by a contract BES-2017-080586. We acknowledge financial support from the grants PGC2018-095862-B-C21, QITEMAD+ S2013/ICE-2801 and SEV-2016-0597 of the ‘‘Centro de Excelencia Severo Ochoa’’ Programme.

- ¹ M. Campos, G. Sierra and E. Lopez, “Tensor renormalization group in bosonic field theory,” *Phys. Rev. B* **100**, 195106 (2019).
- ² I. Affleck, T. Kennedy, E. H. Lieb, and H. Tasaki, “Valence bond ground states in isotropic quantum antiferromagnets”, *Commun. Math. Phys.*, **115**, 477 (1988).
- ³ S. R. White, “Density matrix formulation for quantum renormalization groups”, *Phys. Rev. Lett.* **69**, 2863 (1992).
- ⁴ M. Fannes, B. Nachtergaele, and R. F. Werner, “Finitely correlated states on quantum spin chains”, *Commun. Math. Phys.* **144**, 443 (1992).
- ⁵ A. Klümper, A. Schadschneider, and J. Zittartz “Matrix-product-groundstates for one-dimensional spin-1 quantum antiferromagnets”, *Europhys. Lett.* **24**, 293 (1993).
- ⁶ S. Östlund and S. Rommer, “Thermodynamic Limit of Density Matrix Renormalization”, *Phys. Rev. Lett.* **75**, 3537 (1995).
- ⁷ T. Nishino. “Density Matrix Renormalization Group Method for 2D Classical Models”. *J. Phys. Soc. Jpn.*, **64**, 3598 (1995).
- ⁸ T. Nishino and K. Okunishi, “Corner Transfer Matrix Algorithm for Classical Renormalization Group”, *J. Phys. Soc. Jpn.* **66**, 3040 (1997).
- ⁹ J. Dukelsky, M.A. Martin-Delgado, T. Nishino, G. Sierra, “Equivalence of the Variational Matrix Product Method and the Density Matrix Renormalization Group applied to Spin Chains”, *Europhys. Lett.*, **43**, 457 (1998).
- ¹⁰ G. Sierra and M.A. Martin-Delgado “The Density Matrix Renormalization Group, Quantum Groups and Conformal Field Theory”, *Proceed. Workshop on the Exact Renormalization Group, Faro (Portugal) 1998*, arXiv:cond-mat/9811170.
- ¹¹ G. Vidal, “Efficient Classical Simulation of Slightly Entangled Quantum Computations”, *Phys. Rev. Lett.* **91**, 147902 (2003).
- ¹² F. Verstraete, D. Porras, and J. I. Cirac, “DMRG and periodic boundary conditions: a quantum information perspective”, *Phys. Rev. Lett.* **93**, 227205 (2004).
- ¹³ F. Verstraete and J. I. Cirac, “Renormalization algorithms for Quantum-Many Body Systems in two and higher dimensions”, arXiv:cond-mat/0407066v1 (2004).
- ¹⁴ U. Schollwöck, “The density-matrix renormalization group”, *Rev. Mod. Phys.* **77**, 259 (2005).
- ¹⁵ V. Murg, F. Verstraete, and J. I. Cirac. “Efficient evaluation of partition functions of frustrated and inhomogeneous spin systems”. *Phys. Rev. Lett.*, **95**, 057206 (2005).
- ¹⁶ D. Pérez-García, F. Verstraete, M. M. Wolf, J. I. Cirac, “Matrix product state representations”, *Quantum Inf. Comput.* **7**, 401 (2007).
- ¹⁷ M. Levin and C. P. Nave, “Tensor Renormalization Group Approach to Two-Dimensional Classical Lattice Models”, *Phys. Rev. Lett.* **99**, 120601 (2007).
- ¹⁸ G. Vidal, “Entanglement Renormalization”, *Phys. Rev. Lett.* **99**, 220405 (2007).
- ¹⁹ V. Giovannetti, S. Montangero, R. Fazio, “Quantum MERA Channels”, *Phys. Rev. Lett.* **101**, 180503 (2008).
- ²⁰ F. Verstraete, J.I. Cirac, V. Murg, “Matrix Product States, Projected Entangled Pair States, and variational renormalization group methods for quantum spin systems”, *Adv. Phys.* **57**, 143 (2008).
- ²¹ R. N. C. Pfeifer, G. Evenbly, and G. Vidal, “Entanglement renormalization, scale invariance, and quantum criticality”, *Phys. Rev. A* **79**, 040301 (2009).
- ²² Z.-C. Gu and X.-G. Wen, “Tensor-entanglement-filtering renormalization approach and symmetry-protected topological order”, *Phys. Rev. B* **80**, 155131 (2009).
- ²³ F. Pollmann, A. M. Turner, E. Berg, and M. Oshikawa, “Entanglement spectrum of a topological phase in one dimension”, *Phys. Rev. B* **81**, 064439 (2010).
- ²⁴ X. Chen, Z.-C. Gu, and X.-G. Wen, “Classification of gapped symmetric phases in one-dimensional spin systems”, *Phys. Rev. B* **83**, 035107 (2011).
- ²⁵ N. Schuch, D. Pérez-García, and J. I. Cirac, “Classifying quantum phases using matrix product states and projected entangled pair states”, *Phys. Rev. B* **84**, 165139 (2011).
- ²⁶ Y. Shimizu, “Tensor renormalization group approach to a lattice boson model”, *Mod. Phys. Lett. A* **27**, 1250035 (2012).
- ²⁷ R. Orús, “A practical introduction to tensor networks: Matrix product states and projected entangled pair states”, *Ann. Phys.* **349**, 117 (2014).
- ²⁸ G. Evenbly and G. Vidal, “Tensor Network Renormalization”, *Phys. Rev. Lett.* **115**, 180405 (2015).
- ²⁹ G. Evenbly and G. Vidal, “Tensor network renormalization yields the multi-scale entanglement renormalization ansatz”, *Phys. Rev. Lett.* **115**, 200401 (2015).
- ³⁰ S.-J. Ran, C. Peng, W. Li, M. Lewenstein, G. Su, “Criticality in Two-Dimensional Quantum Systems: Tensor Network Approach”, *Phys. Rev. B* **95**, 155114 (2017).
- ³¹ M. Bal, M. Mariën, J. Haegeman, F. Verstraete, “Renormalization group flows of Hamiltonians using tensor networks” *Phys. Rev. Lett.* **118**, 250602 (2017).
- ³² H. He, Y. Zheng, B. Andrei Bernevig, N. Regnault, “Entanglement Entropy From Tensor Network States for Stabilizer Codes”, *Phys. Rev. B* **97**, 125102 (2018).
- ³³ S. Singha Roy, H. Shekhar Dhar, A. Sen De, U. Sen, “Tensor-network approach to compute genuine multisite entanglement in infinite quantum spin chains”, *Phys. Rev. A* **99**, 062305 (2019).
- ³⁴ M. C. Banuls, K. Cichy, H.-T. Hung, Y.-J. Kao, C.-J. D. Lin, Y.-P. Lin, D. T.-L. Tan, “Phase structure and real-time dynamics of the massive Thirring model in 1+1 dimensions using the tensor-network method”, *PoS (LATTICE2019)* 022.
- ³⁵ D. Kadoh, Y. Kuramashi, Y. Nakamura, R. Sakai, S. Takeda and Y. Yoshimura, “Tensor network analysis of critical coupling in two dimensional ϕ^4 theory”, *JHEP* **05** (2019), 184.
- ³⁶ B. Vanhecke, J. Haegeman, K. Van Acoleyen, L. Vanderstraeten, F. Verstraete, “A scaling hypothesis for matrix product states”, *Phys. Rev. Lett.* **123**, 250604 (2019).
- ³⁷ J. Garre-Rubio, “Symmetries in topological tensor network states: classification, construction and detection”, arXiv:1912.08597.
- ³⁸ M. C. Banuls, M. P. Heller, K. Jansen, J. Knaute, V. Svensson, “From spin chains to real-time thermal field theory using tensor networks”, *Phys. Rev. Research* **2**, 033301 (2020).
- ³⁹ Hui-Ke Jin, Hong-Hao Tu, Yi Zhou, “Efficient tensor network representation for Gutzwiller projected states of paired fermions”, *Phys. Rev. B* **101**, 165135 (2020).
- ⁴⁰ C. Delcamp, A. Tilloy, “Computing the renormalization group flow of two-dimensional ϕ^4 theory with tensor networks”, *Phys. Rev. Research* **2**, 033278 (2020);
- ⁴¹ Q. Mortier, N. Schuch, F. Verstraete, J. Haegeman, “Resolving Fermi surfaces with tensor networks”, arXiv:2008.11176.
- ⁴² D. Poilblanc, M. Mambrini, F. Alet, “Finite-temperature symmetric tensor network for spin-1/2 Heisenberg antiferromagnets on the square lattice”, *SciPost Phys.* **10**, 019 (2021).
- ⁴³ B. Vanhecke, F. Verstraete, K. Van Acoleyen, “Entanglement scaling for $\lambda\phi_2^4$ ”, arxiv.2104.10564.
- ⁴⁴ F. Verstraete and J. I. Cirac, “Continuous matrix product states for quantum fields”, *Phys. Rev. Lett.* **104**, 190405 (2010).

- ⁴⁵ J. Haegeman, T. J. Osborne, H. Verschelde and F. Verstraete, “Entanglement renormalization for quantum fields in real space”, Phys. Rev. Lett. **110**, 100402 (2013).
- ⁴⁶ D. Jennings, C. Brockett, J. Haegeman, T. J. Osborne and F. Verstraete, “Continuum tensor network field states, path integral representations and spatial symmetries”, New J. Phys. **17**, 063039 (2015).
- ⁴⁷ A. Tilloy, J. I. Cirac “Continuous Tensor Network States for Quantum Fields”, Phys. Rev. X **9**, 021040 (2019)
- ⁴⁸ J. Cotler, M. R. M. Mozaffar, A. Mollabashi, A. Naseh, “Renormalization Group Circuits for Weakly Interacting Continuum Field Theories”, Fortschr. Phys. **67**, 1900038 (2019).
- ⁴⁹ Q. Hu, A. Franco-Rubio, G. Vidal, “Continuous tensor network renormalization for quantum fields”, arXiv:1809.05176.
- ⁵⁰ T. D. Karanikolaou, P. Emonts, A. Tilloy, “Gaussian Continuous Tensor Network States for Simple Bosonic Field Theories” Phys. Rev. Research **3**, 023059 (2021). arXiv:2006.13143.
- ⁵¹ A.E. B. Nielsen, B. Herwerth, J. I. Cirac, and G. Sierra, “Field tensor network states”, Phys. Rev. B **103**, 155130 (2021).
- ⁵² B. Swingle, “Entanglement renormalization and holography”, Phys. Rev. D **86**, 065007 (2012).
- ⁵³ J. I. Latorre and G. Sierra, “Holographic codes”, arXiv:1502.06618.
- ⁵⁴ F. Pastawski, B. Yoshida, D. Harlow, and John Preskill, “Holographic quantum error-correcting codes: toy models for the bulk/boundary correspondence”, J. High Energy Phys. **2015**, **149**, (2015).
- ⁵⁵ J. Molina-Vilaplana, “Information geometry of entanglement renormalization for free quantum fields”, J. High Energy. Phys. **2015**, 2 (2015).
- ⁵⁶ M. Miyaji, T. Numasawa, N. Shiba, T. Takayanagi, K. Watanabe, “cMERA as Surface/State Correspondence in AdS/CFT”, Phys. Rev. Lett. **115**, 171602 (2015).
- ⁵⁷ P. Caputa, N. Kundu, M. Miyaji, T. Takayanagi, and K. Watanabe, “Liouville action as path-integral complexity: from continuous tensor networks to AdS/CFT”, J. High Energy Phys. **2017**, **97** (2017).
- ⁵⁸ R. Vasseur, A. C. Potter, Y.-Z. You, A. W. W. Ludwig, “Entanglement Transitions from Holographic Random Tensor Networks”, Phys. Rev. B **100**, 134203 (2019).
- ⁵⁹ A. Jahn, J. Eisert, “Holographic tensor network models and quantum error correction: A topical review”, arXiv:2102.02619.
- ⁶⁰ <https://github.com/m-campos/interacting-trg>.
- ⁶¹ K.G. Wilson, “Group and Critical Phenomena. I. Renormalization Group and the Kadanoff Scaling Picture”, Phys. Rev. B **4**, 3174 (1971).
- ⁶² R. Shankar, “Renormalization Group Approach to Interacting Fermions”, Rev. Mod. Phys. **66**, 129 (1994).
- ⁶³ M. Abramowitz, I. A. Stegun, *Handbook of Mathematical Functions with Formulas, Graphs, and Mathematical Tables*. Applied Mathematics Series **55**, New York, Dover Publications (1970).

Appendix A: SVD vs gaussian SVD

In this appendix we compare the standard SVD with the gaussian SVD employed throughout the paper as the basic mathematical tool to implement the gTRG. The SVD is equivalent to the Schmidt decomposition of a quantum state. We shall use this correspondence in what follows.

1. The Fourier transform as a continuous SVD

Let us start with eq.(11)

$$e^{-\frac{1}{2}(x_1-x_2)^2} = \int \frac{dp}{\sqrt{2\pi}} e^{ip(x_1-x_2) - \frac{1}{2}p^2}, \quad (\text{A1})$$

and define the state

$$|\psi\rangle = \int dx_1 dx_2 e^{-\frac{1}{2}(x_1-x_2)^2} |x_1\rangle \otimes |x_2\rangle, \quad (\text{A2})$$

where $|x\rangle$ is a orthonormal basis in the Dirac sense, that is $\langle x|x'\rangle = \delta(x-x')$. Eq.(A2) represents a pair of particles in a bound state that using (A1) can be written as

$$|\psi\rangle = \sqrt{2\pi} \int dp e^{-\frac{1}{2}p^2} |p\rangle \otimes |-p\rangle, \quad (\text{A3})$$

where the states

$$|p\rangle \equiv \int \frac{dx}{\sqrt{2\pi}} e^{ipx} |x\rangle, \quad (\text{A4})$$

satisfy

$$\langle p|p'\rangle = \delta(p-p'). \quad (\text{A5})$$

Eq.(A3) is the Schmidt decomposition of the state (A2) in the orthonormal basis $|p\rangle$. Eq. (A1) is a continuous SVD, that is nothing but the Fourier transform of $e^{-\frac{1}{2}p^2}$. Notice that the norm of (A3) is $\langle \psi|\psi\rangle = 2\pi^{3/2}\delta(0)$ that reflects the translational invariance of the two body wave function $e^{-\frac{1}{2}(x_1-x_2)^2}$.

2. SVD of a normalized gaussian state

Let us next consider the function

$$W(x_1, x_2) = \rho e^{-\frac{a}{2}(x_1^2 + x_2^2) + bx_1 x_2}, \quad (\text{A6})$$

that has the same form as eq.(12). We define the state

$$|W\rangle = \int dx_1 dx_2 W(x_1, x_2) |x_1\rangle \otimes |x_2\rangle, \quad (\text{A7})$$

that is normalized provided $a > |b|$, with the normalization factor $\rho = \pi^{-1/2}(a^2 - b^2)^{1/4}$. The state (A2) corresponds to $a = b = 1$ that, as explained above, is normalized in the Dirac sense.

To find the Schmidt decomposition of (A7) we use the identity⁶³

$$\sum_{n=0}^{\infty} \frac{u^n}{2^n n!} H_n(x) H_n(y) = \frac{1}{\sqrt{1-u^2}} \exp\left(\frac{2u}{1+u}xy - \frac{u^2}{1-u^2}(x-y)^2\right), \quad (\text{A8})$$

where $H_n(x)$ are the Hermite polynomials that give the eigenfunctions of the Hamiltonian of the harmonic oscillator $H = \frac{1}{2}(-\partial_x^2 + x^2)$,

$$\psi_n(x) = \frac{1}{\sqrt{\pi^{1/2} 2^n n!}} H_n(x) e^{-x^2/2}. \quad (\text{A9})$$

Using (A9) one can write (A8) as

$$\sum_{n=0}^{\infty} u^n \psi_n(x) \psi_n(y) = \frac{1}{\sqrt{\pi(1-u^2)}} \exp\left(-\frac{x^2 + y^2 - 2uxy}{2(1-u^2)}\right). \quad (\text{A10})$$

Comparing (A6) and (A10) we find

$$ax_1^2 = \frac{x^2}{1-u^2}, \quad ax_2^2 = \frac{y^2}{1-u^2}, \quad bx_1 x_2 = \frac{uxy}{1-u^2}, \quad (\text{A11})$$

so that

$$u^2 = \left(\frac{b}{a}\right)^2. \quad (\text{A12})$$

Let us write (A6) using the variables x and y

$$W(x, y) = \frac{1}{\sqrt{\pi}} \exp\left(-\frac{x^2 + y^2 - 2uxy}{2(1-u^2)}\right), \quad |u| < 1 \quad (\text{A13})$$

where we took into account the Jacobian of the transformation. The state (A7) becomes

$$|W\rangle = \sqrt{1-u^2} \sum_{n=0}^{\infty} u^n |n\rangle \otimes |n\rangle, \quad (\text{A14})$$

where

$$|n\rangle = \int dx \psi_n(x) |x\rangle. \quad (\text{A15})$$

Equation (A14) is the Schmidt decomposition of $|W\rangle$ in terms of the discrete Schmidt coefficients,

$$w_n = \sqrt{1-u^2} u^n, \quad u = 0, 1, \dots, \infty. \quad (\text{A16})$$

Taking the trace over the left, or right, Hilbert space of the pure density matrix of (A14) gives

$$\rho = \text{tr}_L |W\rangle \langle W| = (1-u^2) \sum_{n=0}^{\infty} u^{2n} |n\rangle \langle n| \quad (\text{A17})$$

whose von Neumann entropy is

$$S_1 = -\log(1-u^2) - \frac{u^2 \log u^2}{1-u^2}, \quad (\text{A18})$$

that diverges in the limit $u^2 \rightarrow 1^-$.

3. Gaussian SVD of a normalized gaussian state

Let us consider again the state (A7), and write (A6) as

$$W(x_1, x_2) = \rho e^{-\frac{1}{2}(a-b)(x_1^2+x_2^2) - \frac{b}{2}(x_1-x_2)^2}. \quad (\text{A19})$$

Using (A1) with $x_{1,2} \rightarrow \sqrt{b}x_{1,2}$, this equation reads

$$W(x_1, x_2) = \rho e^{-\frac{1}{2}(a-b)(x_1^2+x_2^2)} \int \frac{dp}{\sqrt{2\pi b}} e^{ip(x_1-x_2) - \frac{1}{2b}p^2}, \quad (\text{A20})$$

that allow us to write (A7) as

$$|W\rangle = \frac{\rho}{\sqrt{2\pi b}} \int dp e^{-\frac{1}{2b}p^2} |p, a-b\rangle \otimes |-p, a-b\rangle, \quad (\text{A21})$$

where

$$|p, a-b\rangle = \int dx e^{-\frac{1}{2}(a-b)x^2 + ipx} |x\rangle. \quad (\text{A22})$$

These states are not orthogonal since

$$\langle p, a-b | p', a-b \rangle = \sqrt{\frac{\pi}{a-b}} e^{-\frac{(p-p')^2}{4(a-b)}}. \quad (\text{A23})$$

Equation (A21) looks like a continuous Schmidt decomposition similar to (A3), but it is not because the basis $|p, a-b\rangle$ is not orthogonal when $a > |b|$. On the other hand, we saw above that the Schmidt decomposition of $|W\rangle$ involves an infinite number of terms but is discrete (see (A14)). The gaussian SVD is an example of a look alike Schmidt decomposition that is forced upon us by the condition of working with the exponent of the Boltzmann weights or the effective action in Quantum Field Theory.

Appendix B: Loop matrices

We will construct the matrices Q_n and C_n that govern the gaussian kernel of the TRG coarse graining integrals. The leading gaussian terms do not couple the fields with a counterpart in the free model, the set (66), with the new fields (67) introduced by interaction. For the $n = 2$ matrices, this was made explicit in (63). Based on it, we will focus on the matrix blocks associated with the set (66). They are given by the same expressions that apply to the free network. In order to simplify notation, we refer to the free case in the following presentation.

In an appropriate basis, and up to a proportionality constant, the Boltzmann weights of the free model are described by

$$\begin{array}{c|c} \mathbf{x}_2 & \mathbf{x}_3 \\ \hline \mathbf{x}_1 & \mathbf{x}_4 \end{array} = e^{-\frac{1}{2}\mathbf{x}M_n\mathbf{x}}, \quad M_n = \begin{pmatrix} A_n & 0 \\ 0 & A_n \end{pmatrix} + \begin{pmatrix} B_n & -B_n \\ -B_n & B_n \end{pmatrix}. \quad (\text{B1})$$

The 2×2 block structure of M_n corresponds to the choice $\mathbf{x} = (\mathbf{x}_L, \mathbf{x}_R)$ with $\mathbf{x}_L = (\mathbf{x}_1, \mathbf{x}_2)$ and $\mathbf{x}_R = (\mathbf{x}_4, \mathbf{x}_3)$, motivated by a subsequent splitting of W_n along the axis 12–34. The factorization of the Boltzmann weights is based on the SVD of B_n , which rewrites this matrix as $U_n D_n U_n^T$. In general U_n is a $2\chi_n \times \chi_{n+1}$ isometry. We have $\chi_{n+1} \leq 2\chi_n$, since some singular values in D_n might be truncated because their number is larger than χ_{\max} or discarded because they vanish. The matrices A_n and U_n have a further interesting structure¹

$$A_n = \frac{1}{2} \mathbb{1}_2 \otimes D_{n-1}^{-1} + \begin{pmatrix} a_n & -a_n \\ -a_n & a_n \end{pmatrix}, \quad U_n = \frac{1}{\sqrt{2}} \begin{pmatrix} u_n & v_n \\ u_n & -v_n \end{pmatrix}. \quad (\text{B2})$$

The matrix a_n is real symmetric and positive. Both a_n and D_{n-1} have dimension $\chi_n \times \chi_n$. The isometries u_n and v_n have real entries and dimension $\chi_n \times \frac{1}{2}\chi_{n+1}$, satisfying $u_n^+ u_n = v_n^+ v_n = \mathbb{1}$.

After splitting W_n into two cubic weights according to the 2×2 block structure in (B1), four cubic weights are sewed together in order to obtain W_{n+1} . The kernel of the coarse graining integral that eliminates the fields \mathbf{x} in favour of the next level \mathbf{p} is

$$\mathbf{p}_L = (\mathbf{p}_1, \mathbf{p}_2) \quad \begin{array}{c} \text{2} \quad \text{3} \\ \diagup \quad \diagdown \\ \text{2} \quad \text{4} \\ \diagdown \quad \diagup \\ \text{1} \quad \text{4} \\ \text{1} \end{array} \quad \mathbf{p}_R = (\mathbf{p}_4, \mathbf{p}_3) = e^{-\frac{1}{2}\mathbf{x}Q_n\mathbf{x}+i\mathbf{x}C_n\mathbf{p}}, \quad (\text{B3})$$

$\mathbf{x} = (\mathbf{x}_1, \mathbf{x}_2, \mathbf{x}_3, \mathbf{x}_4)$

where we have ignored again a multiplicative constant. The $4\chi_n \times 4\chi_n$ matrix Q is readily built out of D_{n-1}^{-1} and a_n

$$Q_n = \mathbb{1}_4 \otimes D_{n-1}^{-1} + \begin{pmatrix} 2 & -1 & 0 & -1 \\ -1 & 2 & -1 & 0 \\ 0 & -1 & 2 & -1 \\ -1 & 0 & -1 & 2 \end{pmatrix} \otimes a_n. \quad (\text{B4})$$

It is convenient to decompose the matrix C_n into two components such that $C_n\mathbf{p} = C_{n,L}\mathbf{p}_L + C_{n,R}\mathbf{p}_R$. The $4\chi_n \times 2\chi_{n+1}$ matrices $C_{n,L,R}$ are constructed in terms of the isometries u_n and v_n

$$C_L = \frac{1}{\sqrt{2}} \begin{pmatrix} u_n & v_n & 0 & 0 \\ u_n & -v_n & -u_n & v_n \\ 0 & 0 & -u_n & -v_n \\ 0 & 0 & 0 & 0 \end{pmatrix}, \quad C_R = \frac{1}{\sqrt{2}} \begin{pmatrix} -u_n & -v_n & 0 & 0 \\ 0 & 0 & 0 & 0 \\ 0 & 0 & u_n & v_n \\ -u_n & v_n & u_n & -v_n \end{pmatrix}. \quad (\text{B5})$$

The zeroes in the last row of $C_{n,L}$ reflect that \mathbf{x}_4 does not couple to \mathbf{p}_L and correspondingly for the second row of zeroes in $C_{n,R}$. Generalizing (59) and (63), we obtain

$$A_{n+1} = \frac{1}{2} \left[\mathbb{1}_2 \otimes D_n^{-1} + (C_{n,L} - C_{n,R})^T Q_n^{-1} (C_{n,L} - C_{n,R}) \right], \quad B_{n+1} = -C_{n,L}^T Q_n^{-1} C_{n,R}, \quad (\text{B6})$$

where from (B1) we have used

$$C_{n,L}^T Q_n^{-1} C_{n,L} = C_{n,R}^T Q_n^{-1} C_{n,R}, \quad C_{n,L}^T Q_n^{-1} C_{n,R} = C_{n,R}^T Q_n^{-1} C_{n,L}. \quad (\text{B7})$$

Appendix C: Feynman rules

We present the Feynman rules for building the diagrammatic expansion of F_1 (37)

$$F_1(\mathbf{p}) = \int d\mathbf{x} e^{-\frac{1}{2}\mathbf{x}Q_0\mathbf{x}} \prod_{i=1}^4 f_0^{(i)}(\mathbf{x} + iQ_0^{-1}C_0\mathbf{p}). \quad (\text{C1})$$

In analogy with the Wilsonian effective action reviewed in Section 3, double lines are used to represent the fields integrated over ($\mathbf{x} \equiv$ fast fields) and single lines for the next level fields ($\mathbf{p} \equiv$ slow fields). The propagator of the fast fields is given by

$$i \text{ --- } j \quad (Q_0^{-1})_{ij}, \quad (\text{C2})$$

with $i = 1, \dots, 4$. The kinetic terms and spatial derivatives in the original lagrangian (1) render the matrix Q_0 non-diagonal. As a consequence Q_0^{-1} propagates linear combinations involving all four \mathbf{x} -fields in the integral (C1). On the contrary, interaction in the initial lattice only couples fields living on the same link. Using a $\lambda\phi^4$ theory as example, the interaction vertex for the \mathbf{x} fields is

$$\begin{array}{c} i \quad i \\ \diagdown \quad \diagup \\ \diagup \quad \diagdown \\ i \quad i \end{array} \quad \lambda. \quad (\text{C3})$$

The interaction vertices between fast and slow fields are obtained by dressing some double lines of the vertex (C3) with $Q_0^{-1}C_0$

$$\begin{array}{c} i \\ \diagup \quad \diagdown \\ a \quad i \end{array} \quad \lambda (Q_0^{-1}C_0)_{ia} \quad \begin{array}{c} b \\ \diagup \quad \diagdown \\ a \quad i \end{array} \quad \lambda (Q_0^{-1}C_0)_{ia}(Q_0^{-1}C_0)_{ib} \quad , \quad (C4)$$

and analogously for all other possible replacements of double by single lines. In order to avoid confusion, we use the letters $a, b, \dots = 1, \dots, 8$ to label the \mathbf{p} fields of the level one tilted lattice. Due to the dressing $Q_0^{-1}C_0$, interaction couples \mathbf{p} fields from different lattice links. The interaction vertex of the level one Boltzmann weight W_1 is

$$\begin{array}{c} b \quad c \\ \diagup \quad \diagdown \\ a \quad d \end{array} \quad \lambda \sum_{i=1}^4 (Q_0^{-1}C_0)_{ia}(Q_0^{-1}C_0)_{ib}(Q_0^{-1}C_0)_{ic}(Q_0^{-1}C_0)_{id} \quad . \quad (C5)$$

The Feynman rules for constructing F_n with $n > 1$ are more involved due to the doubling of the splitting fields explained in Section 4.B and the different roles of the fields in the sets (66) and (67). A sketch of the Feynman rules necessary for working at first order in perturbation theory can be found in the readme document of the GitHub link⁶⁰.

Appendix D: A bound on odd fields

Odd variables can contribute to LR mixing via the functions F_n , which contain the effect of interaction on the Boltzmann weights W_n . These functions are given by Hermite-like expressions, with the associated differential operator $\hat{\mathcal{F}}_n$ obtained from an integral generalizing (61)

$$\hat{\mathcal{F}}_n(\bar{\mathbf{x}}, \partial_{\mathbf{u}}) = \int d\mathbf{p} \quad \begin{array}{c} \text{---} \text{---} \text{---} \text{---} \\ \diagup \quad \diagdown \\ \text{---} \quad \text{---} \\ \diagdown \quad \diagup \\ \text{---} \end{array} \quad \begin{array}{c} \hat{f}_{n-1}^{(i)} \\ \nearrow \\ i+1 \\ \text{---} \\ i \\ \searrow \\ \partial_{\mathbf{u}_i} \\ \text{---} \\ (\mathbf{p} + iQ_{n-1}^{-1}C_{n-1}\bar{\mathbf{x}})_i \end{array} \quad . \quad (D1)$$

The arguments of function $\hat{f}_{n-1}^{(i)}$ live at the links intersected by the dotted circle: the shifted fields $\mathbf{p}_{i,i+1}$ and the derivatives $\partial_{\mathbf{u}_i}$. The latter generate a dependence of F_n on $\hat{\mathbf{x}}_i$ after evaluating the corresponding expression (60).

We assume that W_n will be subsequently factorized along the axis $i : (1,2)_L - (3,4)_R$. A generic connected Feynman diagram in the expansion of $\hat{\mathcal{F}}_n$ has the form

$$\begin{array}{c} 1 \\ \diagup \quad \diagdown \\ 2 \quad 1 \\ \text{---} \quad \text{---} \\ \text{---} \quad \text{---} \\ \diagdown \quad \diagup \\ k_L \quad k_R \end{array} \quad \begin{array}{c} m_L \quad m_R \\ \text{---} \quad \text{---} \end{array} \quad \begin{array}{c} 1 \\ \diagup \quad \diagdown \\ 1 \\ \text{---} \quad \text{---} \\ \text{---} \quad \text{---} \\ \diagdown \quad \diagup \\ k_R \end{array} \quad \text{R} : \partial_{\mathbf{u}_{3,4}} \quad . \quad (D2)$$

The subgraph on the left combines diagrams from $\hat{f}_{n-1}^{(i)}$ with $i = 1, 2$ and contributes m_L powers of the coupling constant. It has k_L single line external legs, which can carry any field $\bar{\mathbf{x}}_j$ but only \mathbf{u} -derivatives with indices $i = 1, 2$. The same applies to the subgraph on the right, with $i = 3, 4$, m_R and k_R . When m_L or m_R vanish all derivatives belong to the same L or R side. A symmetric definition of the cubic weights emerging from W_n , namely $V_{n,L} = V_{n,R}$ as in (9), is compatible with assigning a diagram with m_R or $m_L = 0$ to $V_{n,L}$ or $V_{n,R}$ respectively. With this choice, factorization is achieved by just introducing splitting fields for even variables. Hence, odd fields only require their own set of splitting fields in diagrams satisfying

$$m_L, m_R \geq 1, \quad m_L + m_R \leq N, \quad (D3)$$

with N the order at which we want the perturbative expansion to stop.

Appendix E: A bound on even fields

Without truncation, the bond dimension in the free network doubles when progressing from the coarse graining level $2n$ to the level $2n + 1$, but remains the same from $2n + 1$ to $2n + 2$. Namely

$$\chi_{2n+1} = 2\chi_{2n}, \quad \chi_{2n+2} = \chi_{2n+1}. \quad (E1)$$

The reason behind this behaviour is the vanishing of half of the B_{2n+1} singular values¹, which leads to discard automatically the associated splitting fields. This property is lost once χ_{\max} is reached and activates the truncation preventing the bond dimension to further grow.

In the presence of interaction, a field can only be discarded when its contribution to entanglement is small both at the level of the leading gaussian structure and the Feynman graphs. Related to that, in the section V.C we raised the question about the fate of the fields inherited from the free network and related to vanishing singular values of B_{2n+1} . We will now prove that they do not participate in the LR factorization of graphs with m_L or m_R equal to zero in the notation of (D2).

Since we are interested in odd coarse graining levels, the corresponding lattice fields will be of type \mathbf{p} . Analogously to (D1), the differential operator $\hat{\mathcal{F}}_{2n+1}$ is schematically given by

$$\hat{\mathcal{F}}_{2n+1}(\bar{\mathbf{p}}, \partial_{\mathbf{u}}) = \int d\mathbf{x} \quad \begin{array}{c} \partial_{\mathbf{u}} \\ \begin{array}{ccc} 2 & & 3 \\ \diagup & & \diagdown \\ 2 & \text{---} & 4 \\ \diagdown & & \diagup \\ 1 & & 4 \\ \text{L} & & \text{R} \end{array} \\ \end{array} \quad \mathbf{x} + iQ_{2n}^{-1}C_{2n}\bar{\mathbf{p}} \quad . \quad (\text{E2})$$

For definiteness, we consider a Feynman graph in the expansion of $\hat{\mathcal{F}}_{2n+1}$ with $m_R = 0$. Such diagram only traces back to the two cubic weights on the left side of the integrand. Its external legs carry the expressions

$$\begin{array}{c} \text{---} \text{---} \text{---} \\ \diagup \quad \diagdown \\ \text{---} \end{array} \quad m_L \quad \text{---} \quad \partial_{\mathbf{u}_{1,2}}, (Q_{2n}^{-1}C_{2n}\bar{\mathbf{p}})_{1,2,3} \quad . \quad (\text{E3})$$

The subindices 1, 2 of the \mathbf{u} -derivatives refer to the tilted lattice links in (E2), while the subindices 1, 2, 3 in the linear combinations of the $\bar{\mathbf{p}}$ fields allude to the corresponding internal links. Contrary to the \mathbf{u} -derivatives, these linear combinations involve fields from the L and R sides and are the only source of LR cross terms in (E3). The leading gaussian structure does not mix the fields which have a counterpart in the free network, the set (66), with the fields (67) required to keep the TRG manipulations local. Therefore although both appear in the previous linear combinations, we can treat them separately. Using this, in the following we focus on the former and disregard the latter.

It is natural to assign the graph (E3) to the cubic vertex $V_{2n+1,L}$. The dependence on $\bar{\mathbf{p}}_R$ should be thus eliminated as explained in Section IV.B. It results in the substitution

$$Q_{2n}^{-1}C_{2n}\bar{\mathbf{p}} = Q_{2n}^{-1}(C_{2n,L}\bar{\mathbf{p}}_L + C_{2n,R}\bar{\mathbf{p}}_R) \longrightarrow Q_{2n}^{-1}[(C_{2n,L} + C_{2n,R})\bar{\mathbf{p}}_L + iC_{2n,R}U_{2n+1}\partial_{\mathbf{x}^1}] \quad . \quad (\text{E4})$$

All the matrices here are given by the expressions in Appendix B. In particular $C_{2n,L}$ and $C_{2n,R}$ are constructed in terms the matrices u_{2n} and v_{2n} obtained from the SVD of B_{2n} . Relations (E1) imply that in the absence of truncation, B_{2n} has maximal rank and thus u_{2n} and v_{2n} are orthogonal matrices instead of just isometries. In that case we have

$$C_{2n,L}C_{2n,L}^T = \begin{pmatrix} 1 & 0 & 0 & 0 \\ 0 & 2 & 0 & 0 \\ 0 & 0 & 1 & 0 \\ 0 & 0 & 0 & 0 \end{pmatrix} \otimes \mathbb{1}_{\chi_{2n}} \quad . \quad (\text{E5})$$

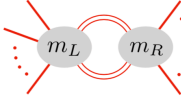
The 4×4 matrix in the *rhs* refers to the four internal links in the integrand of (E2). It has rank three because $C_{2n,L}$ does not couple the fields on the left external links with those on the fourth internal link. Let \mathbf{v} be a singular vector of B_{2n+1} with zero singular value. Multiplying (B6) by $C_{2n,L}$, we obtain

$$(Q_{2n}^{-1}C_{2n,R}\mathbf{v})_{1,2,3} = 0 \quad . \quad (\text{E6})$$

The rows of the matrix U_{2n+1} on the *rhs* of (E4) contain the singular vectors of B_{2n+1} . Let y^1 denote the component of \mathbf{x}^1 related to \mathbf{v} . The previous equality implies that y^1 decouples from the contribution of the graph (E3) to the cubic vertex $V_{2n+1,L}$.

At first order in perturbation theory $m_L + m_R = 1$, and thus m_L or m_R must be zero. We chose again to assign the associated Feynman diagram to the L or R cubic weights respectively. The splitting fields related to vanishing singular values of B_{2n+1} can then be safely ignored. Therefore at first order in λ , the fields (66) and their leading order gaussian structure coincides precisely with those of the free network.

Let us finally consider a generic Feynman diagram in the expansion of $\hat{\mathcal{F}}_{2n+1}$. Its external legs can carry

$$\partial_{\mathbf{u}_{1,2}}, (Q_{2n}^{-1} C_{2n} \bar{\mathbf{p}})_{1,2,3} \longleftarrow \text{Diagram} \longrightarrow \partial_{\mathbf{u}_{3,4}}, (Q_{2n}^{-1} C_{2n} \bar{\mathbf{p}})_{1,3,4} . \quad (\text{E7})$$


If this diagram contributes to $V_{2n+1,L}$, the following term will appear in some of its external legs

$$[(Q_{2n}^{-1} C_{2n,R} \mathbf{v})_4] \partial_{y^1} . \quad (\text{E8})$$

The zero singular value of \mathbf{v} does not impose the vanishing of the combination in brackets. Hence, although y^1 is irrelevant for (E3), it can be important to transmit the entanglement created by the general graph (E7). In that case the field y^1 should not be truncated. Analogous reasoning holds for y^2 , the component of \mathbf{x}^2 related to \mathbf{v} , when a general graph contributes to $V_{2n+1,R}$. The even combination $\bar{y} = y^1 + y^2$ will enlarge then the set of fields (66) beyond those present in the free model.